# Autophagy-related protein Atg11 preserves asymmetric inheritance of spindle microtubule-organizing centers

**Md. Hashim Reza[1], Jigyasa Verma[1$], Ratul Chowdhury[2], Ravi Manjithaya[3], and Kaustuv Sanyal[1, 4*]**

[1]Molecular Mycology Laboratory, Molecular Biology and Genetics Unit, Jawaharlal Nehru Centre for Advanced Scientific Research, Jakkur, Bangalore 560 064, India.

[2]Department of Systems Biology, Harvard Medical School, Boston, MA 02115, USA.

[3]Autophagy Laboratory, Molecular Biology and Genetics Unit, Jawaharlal Nehru Centre for Advanced Scientific Research, Jakkur, Bangalore 560 064, India.

[4]Osaka University, Suita, Osaka, Japan

*Corresponding author: Molecular Mycology Laboratory, Molecular Biology and Genetics Unit, Jawaharlal Nehru Centre for Advanced Scientific Research, Jakkur, Bangalore 560 064, India. Phone: +91 80 2208 2878, e-mail: sanyal@jncasr.ac.in

[$]Present address: Department of Cellular and Physiological Sciences, University of British Columbia, Vancouver, BC, Canada.

**Major Category:** Biological Sciences

**Minor Category:** Genetics/ Cell Biology

**Keywords:** chromosome segregation, SPB asymmetry, spindle position checkpoint, motor proteins, septins

**Abstract**

Asymmetric spindle pole body (SPB) inheritance requires a cascade of events that involve kinases, phosphatases and structural scaffold proteins including molecular motors and microtubule-associated proteins present in the nucleus and/or the cytoplasm. Higher levels of an SPB component Spc72 and the spindle positioning factor Kar9 at the old SPB, which migrates to the daughter cell, ensure asymmetric SPB inheritance. Timely SPB duplication followed by its asymmetric inheritance is a key to correct spindle alignment leading to high-fidelity chromosome segregation. By combining *in silico* analysis of known protein-protein interactions of autophagy (Atg)-related proteins with those that constitute the chromosome segregation machinery, and growth dynamics of 35 *atg* mutants in the presence of a microtubule poison, we identified Atg11 as a potential regulator of chromosome transmission. Cells lacking Atg11 did not show any kinetochore defects but displayed a high rate of chromosome loss and delayed anaphase onset. Atg11 positively interacted with Kar9 and Kip2 and negatively with Dyn1 and Kar3 in mediating proper chromosome segregation suggesting a role of Atg11 in spindle positioning. Indeed, *atg11*Δ cells displayed an inverted SPB inheritance. We further show that Atg11 promotes asymmetric localization of Spc72 and Kar9 on the old SPB. Atg11 physically interacted with Spc72 and transiently localized close to the old SPB during metaphase-to-anaphase progression. Taken together, our study uncovers an autophagy-independent role of Atg11 in spindle alignment and emphasizes the importance of unbiased screens to identify factors mediating the complex and intricate crosstalk between processes fundamental to genomic integrity.

## Significance statement

Dysregulation in spindle alignment during cell division causes decreased lifespan and contributes to diseased states related to aneuploidy such as cancer. The alignment of the mitotic spindle along the mother-bud axis in the budding yeast relies on the differential distribution of proteins between existing old and freshly formed new spindle pole bodies (SPBs). Non-random distribution of Spc72 and Kar9 facilitates the asymmetric inheritance of SPBs, vital for proper spindle elongation and alignment. Here, we identified a non-canonical role of an autophagy-related protein Atg11 in the Kar9-mediated spindle positioning and faithful chromosome segregation. Loss of Atg11 leads to randomized Spc72 distribution. Atg11, like other autophagy proteins, is evolutionarily conserved. Thus, this study reiterates the importance of crosstalk among major biological processes.

## Introduction

Asymmetric cell division is a process that is evolutionarily conserved from bacteria to humans. *Saccharomyces cerevisiae* divides asymmetrically producing daughter cells that are distinct from the mother in size, the molecular composition of proteins and organelles, and replicative lifespan (RLS). Before cell division, *S. cerevisiae* undergoes polarized growth to form a bud. The alignment of the mitotic spindle along the predetermined polarity axis is critical for proper nuclear division. In budding yeast, the spatial crosstalk between astral microtubules (aMTs) and cortical cues regulating mitotic spindle alignment along the polarity axis requires the action of two functionally redundant MT-associated pathways. At metaphase, Kar9 mediates the mitotic spindle alignment along the polarity axis at the bud-neck, where it interacts with the plus-end tracking protein Bim1 at one end (1-3), and to Myo2, a type V myosin, on the other (4). The dynein-dependent pathway operates at anaphase and generates pulling forces to orient the nucleus along the polarity axis (5, 6). Mutations in proteins altering the function of either Kar9 or Dyn1 pathway often misalign the spindle (7, 8). While one pathway compensates for the other, loss of both is lethal for the cell (8). Misaligned spindles lead to the activation of spindle position checkpoint (SPOC) (6, 9-11), another surveillance mechanism, which halts the cell cycle and prevents the exit from mitosis by the inhibition of mitotic exit network (MEN) signalling.

Cytoplasmic motor dynein and kinesin-related proteins (KRPs) regulate MT dynamics and spindle positioning and facilitate equal nuclear segregation in the two daughter cells. Kip3 belongs to the kinesin-8/kinesin-13 family and causes MT depolymerization at the more dynamic plus ends of MTs (12). Kip2, a plus-end directed motor, localizes to the spindle pole bodies (SPBs) and has been shown to play a role in the polymerization of cytoplasmic MTs (13). In contrast, Kar3, belonging to the kinesin-14 family, is a less dynamic minus end-directed motor and primarily acts at SPBs. Kar3 is important for depolymerization of both

cytoplasmic and nuclear microtubules and thereby regulates spindle length dynamics at metaphase (14).

Microtubule-organizing centers (MTOCs) are centrosomes in animal cells or SPBs in budding yeast. Each SPB nucleates nuclear and aMTs from its nuclear and cytosolic faces, respectively. MT nucleation is facilitated by the recruitment of the conserved γ-tubulin complex (γTC), composed of Tub4, Spc97 and Spc98 (15-19), onto Spc110 at the inner plaque (20) and Spc72 at the outer plaque or Kar1 at the half-bridge (21-24). Right after SPB duplication, kinase and phosphatases contribute to the establishment and maintenance of SPB asymmetry through a cascade of events, leading to a difference in protein composition, age, and structure between the two SPBs. Two different premises suggest aMT asymmetry stemming from the contribution of extrinsic and intrinsic factors. The Cyclin-dependent kinase (CDK) Cdc28/Cdk1 facilitates the biased recruitment of Spc72 and the γTC at the old SPB during the early cell cycle stage, and later promotes the assembly of the new SPB in the correct order with the recruitment of the outer plaque following the complete assembly of inner plaque (25). This intrinsic asymmetry of SPB core proteins contributes to the aMT asymmetry in the dividing cell.

The evidence of non-random SPB inheritance, wherein the pre-existing (old) SPB and the newly formed SPB migrates to the daughter and mother cell respectively, coupled with spindle orientation during asymmetric cell division was first elucidated in the budding yeast. Cdc5, a Polo-like kinase, localizes to the SPBs and contributes to the timely and sequential recruitment of Spc72 and Kar9, the two major determinants of SPB inheritance (26). The microtubule +end tracking protein (+TIP) Kar9 is found at both the poles during the onset of SPB separation. However, as the cell progresses further in the cell cycle, phosphorylation of Kar9 at the new SPB by Cdk1/Clb4 leads to asymmetric localization of Kar9 at the old SPB, enabling spindle alignment along the polarity axis (27). The Kar9-dependent pathway

represents the extrinsic control of aMT asymmetry (28). Any perturbations in the spindle alignment and consequently in the asymmetric cell division has wide implications ranging from early ageing with a decreased RLS, aneuploidy and cancer, or a failure in embryonic development. Therefore, it is imperative to identify new players contributing to the spindle positioning.

With multiple reports of genetic and/or physical interactions between autophagy and chromosome segregation machinery proteins, the motivation of the present study was to investigate the role of autophagy protein(s) in mediating faithful chromosome segregation in the budding yeast, *S. cerevisiae*, which undergoes closed mitosis. Here, we undertook the screening of *atg* deletion mutants towards microtubule depolymerizing drugs and identified the role of Atg11 in high-fidelity chromosome segregation. Our results uncover a previously unknown autophagy-independent function of Atg11 in mediating asymmetric SPB segregation to help proper spindle alignment during mitosis.

## Results

### Atg11 plays an autophagy-independent role in high-fidelity chromosome transmission

We collated interactions of autophagy proteins with proteins involved in the chromosome segregation machinery using Perl scripts to query the latest curation of the BioGRID yeast interactomes (29) (**Figure 1A**). Subsequently, we carried out a screen to determine the sensitivities of *atg* null mutants to microtubule depolymerizing drug, thiabendazole (TBZ) to confirm the *in silico* predicted interactions. A defect in kinetochore-microtubule interaction enhances the sensitivity of the cell to microtubule depolymerizing drugs as compared to the wild-type. Among the mutants that showed mild to moderate sensitivities to TBZ (**Figure S1A**), *atg11*Δ mutant displayed maximum sensitivity (**Figure 1B**), consistent with an earlier observation (30). An *ATG11*-add back strain in the *atg11*Δ

background complemented the TBZ-induced growth defects suggesting a specific role of *ATG11* towards kinetochore-microtubule interactions (**Figure 1B**). Atg11 displayed three primary interactions in the interaction network including Spc72 and Bud2 which plays a critical role in mitotic spindle alignment and spindle position checkpoint (SPOC) respectively (31, 32) (**Figure 1C**). While *atg11*Δ mutant cells did not show any growth defects at a lower temperature of 14°C (**Figure S1B**), a condition that destabilizes microtubules (33), growth of these mutant cells is severely affected at an elevated temperature of 37°C (**Figure S1B**), that promotes faster microtubule dynamics (34). This was further corroborated by the growth curve of wild-type and *atg11*Δ at 37°C, wherein *atg11*Δ mutant grew significantly slower as compared to the wild-type (**Figure S1C**).

To gain a deeper understanding of the role of Atg11 in chromosome segregation, we studied the rate of chromosome loss by determining the mitotic stability of a linear non-essential chromosome as well as a circular monocentric plasmid. A strain harbouring an extra chromosome carrying the suppressor of the *ade2* mutation displayed a significantly higher rate of chromosome loss in the *atg11*Δ mutant relative to the wild-type grown at 30°C **(Figure 1D**). The loss rate increased further in the *atg11*Δ mutant when grown at 37°C. These results suggest an important but non-essential role of Atg11 in the chromosome segregation in *S. cerevisiae*. Similarly, the average mitotic stability of a monocentric plasmid in *atg11*Δ was found to be significantly lower than the wild-type but comparable to a kinetochore mutant, *ctf19*Δ (**Figure 1E**). Other *atg* mutants tested displayed monocentric plasmid stability similar to that of the wild-type. Loss of Atg1, a protein kinase, leads to abrogation of autophagy (35) and is essential for G2/M to G1 progression under nitrogen starvation conditions (36). Atg17, on the other hand, acts as a scaffold for other Atg proteins and is essential during autophagy induction under starvation conditions. The *atg1*Δ or *atg17*Δ mutant cells did not display any TBZ sensitivity or drop in mitotic stability of the monocentric plasmid as compared to wild-type. Thus, the role

of Atg11 in mediating error-free chromosome segregation is independent of its autophagy function.

**Atg11 is essential for timely anaphase onset**

To gain an insight into the type of defects, we studied the cell cycle progression dynamics of the *atg11*Δ mutant at 30°C and 37°C by FACS. Flow cytometric analysis revealed an increased population of *atg11*Δ mutant at the G2/M stage relative to wild-type at 30°C (**Figure 2A**). Accumulation of *atg11*Δ cells at G2/M further increased when grown at 37°C (**Figure 2A**). The increased percentage of large-budded cells with an unsegregated nucleus having 2N DNA content in the mutant at 37°C indicates the inability of *atg11*Δ cells to segregate chromosomes during mitosis causing G2/M arrest (**Figure 2B**).

Next, we looked at the role of Atg11 in maintaining kinetochore integrity. The *CEN* transcriptional read-through assay suggested that Atg11 does not play any role in the maintenance of the kinetochore ensemble in *S. cerevisiae* (**Figures S2A-B**). Microscopic examination of Tub1-tagged microtubules revealed the proportion of large-budded cells of *atg11*Δ with short, early anaphase spindle (2-4 µm) was two-fold higher compared to the wild-type that was further increased at a higher temperature (**Figures 2C-D**). Subsequently, we examined how the loss of Atg11 affected cell cycle progression. The live-cell imaging using a strain with the marked SPBs (Spc42-mCherry) and the mitotic spindle (GFP-Tub1) revealed that the *atg11*Δ cells accumulated at G1/S and G2/M before progressing into anaphase (**Figures 2E-G**). Similarly, live-cell imaging confirmed a significant delay in the nuclear division in the mutant as compared to the wild-type (**Figure 2H**). This delay in the nuclear division is further exacerbated at 37°C in the *atg11*Δ cells (**Figures S3A-B**). Collectively, these results confirm a role of Atg11 in spindle elongation during anaphase onset critical for faithful chromosome segregation in *S. cerevisiae*.

These results prompted us to examine whether the *atg11*Δ-associated defects are under the surveillance of the spindle assembly checkpoint (SAC) and/or SPOC. Cells of *atg11*Δ *mad2*Δ double mutant were conditionally synthetic lethal in the presence of TBZ or under conditions that compromised spindle dynamics (**Figure 3A**). The *atg11*Δ *bub2*Δ double mutant, on the other hand, did not show any significant difference in growth at a higher temperature when compared to the *bub2*Δ mutant (**Figure 3B**). However, the *atg11*Δ *bub2*Δ double mutant was conditionally synthetic lethal in comparison to the *bub2*Δ mutant in the presence of TBZ (**Figure 3B**). FACS analysis revealed that the *atg11*Δ mutant had a significantly lower percentage of G1 cells compared to the wild-type at 30°C and an increased percent of cells at G2/M (**Figure 3C**). At the elevated temperature, the accumulation of G1 cells, but not G2/M cells, was more significant in the *atg11*Δ mutant as compared to the wild-type (**Figure 3C**). Importantly, *atg11*Δ *bub2*Δ double mutant cells but not *atg11*Δ *mad2*Δ, displayed a bypass of arrest, with the cell cycle profile similar to wild-type and *bub2*Δ mutant both at 30°C and 37°C (**Figure 3D**). Taken together, these results strongly indicate the delay in anaphase onset in the *atg11*Δ mutant to be under SPOC surveillance.

**Atg11 helps in spindle alignment by interacting with molecular motors, microtubule-associated proteins (MAPs) and microtubule plus-end tracking proteins (+ TIPs)**

Having established the role of Atg11 in spindle elongation, we sought to understand its genetic interactions with known regulators of spindle elongation. Towards this end, we assayed for genetic interaction for Atg11 with plus and minus-end directed motors, MAPs and + TIPs (Kar9, Bim1, and Cik1), and Atg11 interacting proteins (Iml3, Msi1, and Mcm16) and looked at cellular fitness under various conditions known to modulate spindle stability (**Figures S4A-4B**). The *atg11*Δ *kar3*Δ, *atg11*Δ *cik1*Δ, and *atg11*Δ *dyn1*Δ double mutants displayed a negative genetic interaction, evident by enhanced growth defects at elevated temperature in the presence

or absence of TBZ when compared to their respective null mutants (**Figure 4A**). A significantly increased proportion of metaphase large-budded cells was found to have shorter spindles (2-4 µm) in the *atg11*Δ *kar3*Δ double mutant compared to the *kar3*Δ mutant at 37°C which further corroborated the growth defects observed (**Figure S4C**).

The *atg11*Δ *kip2*Δ, *atg11*Δ *bim1*Δ and *atg11*Δ *kar9*Δ double mutants grew better than their respective null mutants in presence of TBZ suggesting a positive genetic interaction (**Figures 4A and S4B**). Better growth in the presence of TBZ was further supported by an increased percent of post-metaphase cells having late anaphase spindle in the *atg11*Δ *kip2*Δ double mutant treated with TBZ in comparison to the *kip2*Δ mutant (**Figure S4D**). Remarkably, Atg11 displayed positive genetic interactions with plus-end directed motor or (+) TIPs while it showed negative genetic interactions with minus-end directed motors. Both Kip2 and Kar3, via their involvement in cytoplasmic microtubule dynamics, and Dyn1 and Kar9 are known to contribute to spindle positioning in budding yeast. Taken together, our results suggest that Atg11 plays a role in mediating correct spindle positioning together with the cytosolic motors and MAPs known to play a role in spindle positioning at the SPBs (**Figure 4B**).

To investigate whether Atg11 influences the Kar9- or dynein-dependent pathway of spindle positioning, we examined the effect of low temperature, known to enhance the binucleate phenotype (6), on the spindle position that in turn regulates nuclear segregation. The *dyn1*Δ, *kip2*Δ, and *dyn1*Δ *kip2*Δ double mutant strains exhibited a significant increase in the proportion of binucleate cells as reported earlier (13). The *atg11*Δ mutant exhibited a marginal spindle positioning defect (**Figure 4C**). Remarkably, the *atg11*Δ *dyn1*Δ double mutant not only had a significantly increased proportion of binucleated cells but also displayed mitotic exit with mispositioned spindles, marked by the accumulation of multinucleate and anucleate cells (**Figure 4C**). This suggests that Atg11 prevents mitotic exit in cells with mispositioned spindles. Conversely, both *kar9*Δ mutant and *atg11*Δ *kar9*Δ double mutant also displayed a

significant increase in binucleated cells (**Figure 4C**), with no apparent difference between them, suggesting that Atg11 contributes to spindle positioning dependent on Kar9.

**Atg11 maintains the asymmetrical distribution of Spc72 to ensure proper SPB inheritance**

Having established the participation of Atg11 in Kar9-dependent spindle positioning, we sought to address whether loss of *ATG11* leads to any perturbation in the alignment and migration of metaphase spindles close to the bud-neck. The *atg11*Δ mutant had a marginal but significantly higher angle of alignment of the spindle than the wild-type (**Figure 5A**). The *atg11*Δ *kar9*Δ double mutant also displayed a significantly higher angle of alignment similar to the *kar9*Δ mutant (**Figure 5A**), which is known to have this defect (37). Next, we also looked at the position of the metaphase spindle in the mother cell. The *atg11*Δ mutant displayed a significantly lower percentage of cells having metaphase spindle at the bud-neck when compared to the wild-type, which decreased further in the *kar9*Δ mutant (**Figure S5A**), as shown earlier (38). The *atg11*Δ *kar9*Δ double mutant exhibited a significant increase in the proportion of cells having the metaphase spindle at the neck region compared to the *kar9*Δ mutant (**Figure S5A**). Importantly, our analysis of the mispositioned mid-anaphase spindle (4-7 µm) in these mutants suggested that Atg11 does not contribute to anaphase spindle positioning (**Figure S5B**). Collectively, these results confirm the participation of Atg11 in Kar9-dependent metaphase spindle positioning.

The Kar9 pathway also specifies SPB inheritance, with the old SPB oriented towards the daughter cell (39). To investigate the status of SPB inheritance in the *atg11*Δ mutant, an mCherry tagged Spc42 was used as an indicator of SPB age, as reported previously (40). The *atg11*Δ mutant displayed a two-fold increase in SPB inheritance defects, while *kar9*Δ null mutant, as reported previously (11), showed approximately a three-fold increase relative to the

wild-type (**Figure 5B**). Moreover, the *atg11*Δ *kar9*Δ double mutant displayed *kar9*Δ-like SPB inheritance defect (**Figure 5B**). Notably, the *atg1*Δ mutant, having no autophagy, segregated the SPBs similar to the wild-type, suggesting that the function of Atg11 in the Kar9-pathway mediated SPB inheritance is autophagy-independent (**Figure 5B**).

A previous report on the localization interdependency of Spc72, γ-tubulin complex receptor, and Kar9 onto the SPBs, established Spc72 acting upstream of Kar9 (41), and that the lack of Spc72 severely affected Kar9 loading on the SPBs (26). We determined that the lack of Atg11 significantly randomized the loading of Spc72 and Kar9 on the SPBs (**Figures 5C-E**), as the *atg11*Δ mutant displayed a significantly increased proportion of cells having opposite localization of Spc72 and Kar9 on the SPBs (**Figure 5D**). Strikingly, the loss of *ATG11* significantly impacted the localization of Spc72 onto the old SPB when Kar9 was correctly localized (**Figure 5E**). Taken together, these results suggest that Atg11 facilitates the asymmetric localization of Spc72 and Kar9 on the old SPB necessary for the non-random SPB inheritance in budding yeast.

**Atg11 interacts with Spc72**

To test possible physical interactions between Atg11 and Spc72, we performed the yeast two-hybrid (Y2H) assay. This assay confirmed positive interactions between Atg11 and Spc72 (**Figure 5F**), consistent with the previous work (42). The Y2H assay with Cnm67, a protein of the outer plaque of the SPB, did not show any interactions with Atg11 (**Figure S5C**), suggesting that the spatial position of Atg11 and Spc72 is critical for their physical interactions. We also carried out a flexible protein-protein docking study of Atg11 and Spc72 to identify the possible residues necessary for Atg11-Spc72 interaction using a ClusPro-type algorithm (43) within the OptMAVEn-2.0 docking protocol (44). Analysis of the Spc72 pose, as bound to Atg11, revealed hydrophobic packing of the peptide termini by Leu868 and Leu1004 residues

of Atg11, and electrostatic stabilization of the phosphate group using the positively charged side chain of Asp1001 of Atg11 (**Figure S5D**). Taken together, these results suggest a physical association between Atg11 and Spc72 crucial for the asymmetric Spc72 distribution onto the SPBs. This aids in the non-randomized Kar9 asymmetry and consequently asymmetric SPB inheritance.

**Spatial localization of Atg11 during cell cycle reveals its transient association with SPBs and at the bud-neck region**

Having confirmed the canonical localization of sfGFP-Atg11 onto the vacuolar membrane as a punctate signal at all stages of the cell cycle (**Figure S6A**), we further investigated the localization of Atg11 in a cell that expressed Nup49-mCherry, one of the proteins from central FG nucleoporins. Co-localization studies revealed that sfGFP-Atg11 was associated with the nuclear envelope (NE) in the majority of the anaphase cells (**Figures 6A-B**). The ring-like bud-neck localization of Atg11 during anaphase (**Figure 6A**) was confirmed by its co-localization with a septin protein Shs1 (**Figure S6B**). Time-lapse imaging of a strain co-expressing sfGFP-Atg11 and Spc42-mCherry or H1-mCherry further validated the localization of Atg11 at the bud-neck region (**Figures 6C and S6C**). Atg11 continued to localize at the bud-neck irrespective of the presence of the nucleus at the bud-neck (Type 1) or away from the bud-neck (Type 2) in binucleated cells of *dyn1*Δ mutant (**Figure 6D**). Notably, Atg11 was undetected at the bud-neck when the septin split into two distinct rings in the majority of the cells (**Figure 6E**), suggesting crosstalk between septin ring splitting and Atg11 localization at the bud-neck.

Finally, live-cell imaging of Atg11 and Spc42 (SPBs) in the early anaphase stage revealed proximal localization of Atg11 with the old SPB in a high proportion of the cells (**Figure 6F**). The Atg11 punctum then migrated to the daughter cell and at a later stage

appeared near the new SPB as well (**Figures 6F and S6D**). Taken together, our results confirm the transient association of Atg11 with SPBs, at the bud-neck and open a possibility of its involvement in the septin ring assembly.

## Discussion

In this study, a genome-wide screen identified Atg11 as a potential candidate for chromosome stability. The molecular mechanism underpinning the role of Atg11 in genome stability remained unknown until now. By screening *atg* mutants that show growth inhibition in sublethal concentrations of a microtubule poison accompanied by a high rate of chromosome loss, we identified the temporal role of Atg11 during metaphase-anaphase progression. We further reveal that in the absence of Atg11, cells have an increased proportion of mispositioned spindles as well as a loss in SPB asymmetry due to atypical localization of Spc72 and Kar9. These results hinted at the participation of Atg11 in the Kar9-dependent pathway of spindle positioning. Physical interactions between Atg11 with Spc72, as well as localization of Atg11 proximal to the old SPB, further confirmed the role of Atg11 at the SPBs. Finally, we demonstrated that autophagy-deficient cells do not show an increased rate of chromosome loss. Taking together, we propose that Atg11 performs a non-canonical role in spindle positioning in *S. cerevisiae*.

The plus and minus-end-directed molecular motors function either in concert or antagonistically to regulate the dynamics of microtubules. Kip2, a plus-end-directed motor, antagonizes the function of minus-end-directed motors like Kar3, Dyn1, and Kip3 in regulating the length of cytoplasmic microtubules and contributes to the spindle positioning (13). In this study, we show unanticipated and novel genetic interactions between Atg11 with these proteins. Atg11 displayed positive genetic interactions with MT plus-end proteins and negative with minus-end proteins hinting that Atg11 likely has a role at the SPBs in spindle positioning.

Budding yeast engages Kar9 at metaphase, and Dyn1 at anaphase, to position the spindle along the mother-bud axis. Loss of function of Kar9 or Dyn1 leads to spindle misorientation, with anaphase nuclear division occurring in the mother cell, while cells lacking both are inviable (7, 8). Proteins contributing to spindle positioning in the Kar9 pathway includes Nud1, an SPB component, mitotic exit network (MEN) proteins (Tem1, Cdc15, Dbf2-Dbf20), and Dma1 and Dma2, ubiquitin-protein ligase (38, 45). Our results of cellular fitness and binucleate cell phenotype of *atg11*Δ *dyn1*Δ and *atg11*Δ *kar9*Δ double mutants suggested that Atg11 functions in the Kar9 pathway and adds to the existing list of proteins important for spindle positioning. The results obtained with *atg11*Δ *dyn1*Δ double mutant showing an increased proportion of binucleated cells along with a bypass of mitotic exit is in line with those observed upon deletion of *KIN4* or *DMA1 DMA2* in the *dyn1*Δ mutant background. Thus, Atg11, similar to Kin4, Dma1 and Dma2, prevents mitotic exit in the absence of dynein (45, 46). How Atg11 prevents mitotic exit in cells with a mispositioned spindle remains to be investigated. It remains to be explored whether the overexpression of Atg11, like Dma1 overexpression (45), can rescue the checkpoint defects of cells lacking Bub2 and prevent the cells from re-replicating their DNA. This will substantiate the role of Atg11 in mitotic exit.

Cell cycle-dependent kinases and phosphatases ensure the asymmetric distribution of proteins on the SPBs and facilitate the asymmetric inheritance of SPBs during the cell cycle (8, 40, 47, 48). Atg11 localizing close to the old SPB during metaphase-anaphase transition adds to the list of proteins localizing differentially to the dSPB. Physical association between Atg11-Spc72 and the loss of Spc72 asymmetry upon *ATG11* deletion demonstrated in this study uncovers the role of Atg11 in mediating Spc72 asymmetry. Spc72 acting upstream to Kar9 facilitates asymmetric localization of Kar9, which in turn regulates asymmetric SPB inheritance (26, 39, 49). Loss of either Nud1, MEN components or Spc72 results in SPB inheritance defects along with a loss in cell viability at 37°C (26, 32, 38). A recent study

involving constitutive inverted SPB inheritance also exhibited a subtle loss in cell viability at 37°C, which was attributed to an increased SPOC dependence at elevated temperatures (40). Remarkably, the *atg11*Δ mutant displayed all these defects (**Figure 7A**). We posit that Atg11 could function as an adaptor protein for Spc72. Alternatively, Atg11 can indirectly help other regulators in the asymmetric Kar9 establishment to the dSPB. A recent study reported Cdc5, a polo-like kinase, physically interacting with Spc72 at dSPB during the metaphase-anaphase transition in facilitating the establishment of SPB fate (26). Collectively, our results strongly suggest that Atg11 plays a role in spindle positioning dependent on Kar9 and shares the property of preventing mitotic exit in the presence of spindle mispositioning (**Figure 7A**) (50). The functional significance of inverted SPB inheritance, microtubule dynamics, and loss in cell viability at 37°C remains an exciting area to investigate further.

Besides localizing to the pre-autophagosomal structure (PAS) which is close to the vacuoles (51), Atg11 also co-localizes at the nuclear-vacuolar junction (NVJ) with Nvj1, essential for piecemeal nucleophagy (52). Our study, the first time to our knowledge, shows a cell cycle-dependent localization of Atg11 with the nuclear envelope (NE) and SPBs. A recent study reported Atg11 interacting with Nup159, a cytoplasmic FG nucleoporin, in mediating selective autophagy of nuclear pore complexes (53). The bud-neck localization of sfGFP-Atg11 that seems to be dependent on the septin ring assembly, opens up a new avenue of the possible involvement of Atg11 with septa formation. Although, in a study, a similar ring-like, bud-neck localization of Atg11-GFP in *S. cerevisiae* was observed but the authors neither mentioned nor elaborated the significance (54). The MEN proteins, SPOC proteins, and septins residing at the bud-neck regulate spindle positioning and cytokinesis (55-60). Phosphorylation of the Dbf2/Dbf20 consensus sites (RXXS) in Kar9 promotes correct spindle alignment (38). Notably, the amino acid sequence of Atg11 also displays three Dbf2/Dbf20 consensus sites (RXXS) at Ser100, Ser351, and Ser472 positions (**Figure 7B**). Taken together, the interplay

between Atg11, Dbf2/Dbf20 kinase, and septins remains a significant and fascinating area for future investigation.

Along with autophagy, the cell cycle is an evolutionarily conserved process. Our findings are significant in the light of the emerging role of autophagy in genome stability in cells growing in rich media and cell cycle regulation under starvation conditions (36, 61). Atg11 mediating correct spindle alignment, revealed in this work, opens the possibility to understand further the molecular basis of crosstalk between Atg11, SPB inheritance, and SPOC in faithful chromosome segregation. This is important with increasing pieces of evidence establishing an interplay between errors in the spindle alignment with ageing and aneuploidy leading to the development of cancer and neurodegenerative diseases (40, 62-65).

## Materials and Methods

All the strains used in this study are specified in Supplementary file 1. Primer sequences and the plasmids used for strain construction are specified in Supplementary file 2, and Supplementary file 3 respectively. The yeast strains were grown on YEPD media (yeast extract 1%, peptone 2%, and dextrose 2%) at 30°C unless stated otherwise. For the growth assay in presence of thiabendazole (TBZ), overnight grown cultures of wild-type, autophagy mutants, *ctf19*Δ, *mcm16*Δ, and *ATG11* complemented strains were serially diluted and spotted on YEPD containing 50 µg $mL^{-1}$ and imaged on 2 dpi or 36 h. Details of all of the experimental procedures are given in supplementary information Materials and Methods.

## Competing Interests

The authors declare no competing interests.

## Acknowledgements

We thank D. J. Klionsky, C. Kraft, S. K. Ghosh, S. Bhattacharyya, F. Monje-Casas for sharing yeast strains and vectors, and G. Dey for the valuable comments. We thank N. Nala for his assistance with flow cytometry and B. Suma and K. Jayaram at the imaging facility at JNCASR. Financial support from the DBT-RA Program in Biotechnology and Life Sciences is gratefully acknowledged by MHR. The award of JC Bose Fellowship (JCB/2020/000021), SERB, and JNCASR intramural funding support to KS is acknowledged. This work was also supported by the Department of Biotechnology (DBT) grant in Life Science Research, Education and Training at JNCASR (BT/INF/22/SP27679/2018) and SERB grant (CRG/2019/004892) to RM. JV was supported by intramural financial support from JNCASR. We also thank the members of Molecular Mycology Laboratory for their valuable inputs and comments. Some images were created with BioRender.com.

## Author Contributions

M.H.R. and K.S. designed research; M.H.R. and J.V. performed research; M.H.R., J.V., R.C., and R.M. contributed new reagents/ analytical tools; M.H.R., J.V., and K.S. analyzed the data; M.H.R. and K.S. wrote the paper; K.S. gathered funding and supervised the work.

## References

1. W. S. Korinek, M. J. Copeland, A. Chaudhuri, J. Chant, Molecular linkage underlying microtubule orientation toward cortical sites in yeast. *Science* **287**, 2257-2259 (2000).
2. L. Lee *et al.*, Positioning of the mitotic spindle by a cortical-microtubule capture mechanism. *Science* **287**, 2260-2262 (2000).
3. R. K. Miller, S. C. Cheng, M. D. Rose, Bim1p/Yeb1p mediates the Kar9p-dependent cortical attachment of cytoplasmic microtubules. *Mol Biol Cell* **11**, 2949-2959 (2000).

4. H. Yin, D. Pruyne, T. C. Huffaker, A. Bretscher, Myosin V orientates the mitotic spindle in yeast. *Nature* **406**, 1013-1015 (2000).

5. M. Segal, K. Bloom, Control of spindle polarity and orientation in *Saccharomyces cerevisiae*. *Trends Cell Biol* **11**, 160-166 (2001).

6. E. Yeh, R. V. Skibbens, J. W. Cheng, E. D. Salmon, K. Bloom, Spindle dynamics and cell cycle regulation of dynein in the budding yeast, *Saccharomyces cerevisiae*. *The Journal of cell biology* **130**, 687-700 (1995).

7. Y. Y. Li, E. Yeh, T. Hays, K. Bloom, Disruption of mitotic spindle orientation in a yeast dynein mutant. *Proc Natl Acad Sci U S A* **90**, 10096-10100 (1993).

8. R. K. Miller, M. D. Rose, Kar9p is a novel cortical protein required for cytoplasmic microtubule orientation in yeast. *The Journal of cell biology* **140**, 377-390 (1998).

9. A. Bloecher, G. M. Venturi, K. Tatchell, Anaphase spindle position is monitored by the *BUB2* checkpoint. *Nat Cell Biol* **2**, 556-558 (2000).

10. G. Pereira, T. Hofken, J. Grindlay, C. Manson, E. Schiebel, The Bub2p spindle checkpoint links nuclear migration with mitotic exit. *Mol Cell* **6**, 1-10 (2000).

11. Y. Wang, F. Hu, S. J. Elledge, The Bfa1/Bub2 GAP complex comprises a universal checkpoint required to prevent mitotic exit. *Curr Biol* **10**, 1379-1382 (2000).

12. H. Niederstrasser, H. Salehi-Had, E. C. Gan, C. Walczak, E. Nogales, XKCM1 acts on a single protofilament and requires the C terminus of tubulin. *J Mol Biol* **316**, 817-828 (2002).

13. F. R. Cottingham, M. A. Hoyt, Mitotic spindle positioning in *Saccharomyces cerevisiae* is accomplished by antagonistically acting microtubule motor proteins. *The Journal of cell biology* **138**, 1041-1053 (1997).

14. A. Huyett, J. Kahana, P. Silver, X. Zeng, W. S. Saunders, The Kar3p and Kip2p motors function antagonistically at the spindle poles to influence cytoplasmic microtubule numbers. *J Cell Sci* **111**, 295-301 (1998).

15. D. Farache, L. Emorine, L. Haren, A. Merdes, Assembly and regulation of gamma-tubulin complexes. *Open Biol* **8** (2018).

16. S. Geissler *et al.*, The spindle pole body component Spc98p interacts with the gamma-tubulin-like Tub4p of *Saccharomyces cerevisiae* at the sites of microtubule attachment. *EMBO J* **15**, 3899-3911 (1996).

17. M. Knop, G. Pereira, S. Geissler, K. Grein, E. Schiebel, The spindle pole body component Spc97p interacts with the gamma-tubulin of *Saccharomyces cerevisiae* and functions in microtubule organization and spindle pole body duplication. *EMBO J* **16**, 1550-1564 (1997).

18. J. M. Kollman, A. Merdes, L. Mourey, D. A. Agard, Microtubule nucleation by gamma-tubulin complexes. *Nat Rev Mol Cell Biol* **12**, 709-721 (2011).

19. M. Winey, K. Bloom, Mitotic spindle form and function. *Genetics* **190**, 1197-1224 (2012).

20. M. Knop, E. Schiebel, Spc98p and Spc97p of the yeast gamma-tubulin complex mediate binding to the spindle pole body via their interaction with Spc110p. *EMBO J* **16**, 6985-6995 (1997).

21. U. Gruneberg, K. Campbell, C. Simpson, J. Grindlay, E. Schiebel, Nud1p links astral microtubule organization and the control of exit from mitosis. *EMBO J* **19**, 6475-6488 (2000).

22. M. Knop, E. Schiebel, Receptors determine the cellular localization of a gamma-tubulin complex and thereby the site of microtubule formation. *EMBO J* **17**, 3952-3967 (1998).

23. T. C. Lin, A. Neuner, E. Schiebel, Targeting of gamma-tubulin complexes to microtubule organizing centers: conservation and divergence. *Trends Cell Biol* **25**, 296-307 (2015).

24. G. Pereira, U. Grueneberg, M. Knop, E. Schiebel, Interaction of the yeast gamma-tubulin complex-binding protein Spc72p with Kar1p is essential for microtubule function during karyogamy. *EMBO J* **18**, 4180-4195 (1999).

25. M. Geymonat *et al.*, Orderly assembly underpinning built-in asymmetry in the yeast centrosome duplication cycle requires cyclin-dependent kinase. *Elife* **9** (2020).

26. L. Matellan, J. Manzano-Lopez, F. Monje-Casas, Polo-like kinase acts as a molecular timer that safeguards the asymmetric fate of spindle microtubule-organizing centers. *Elife* **9** (2020).

27. M. Meziane, R. Genthial, J. Vogel, Kar9 symmetry breaking alone is insufficient to ensure spindle alignment. *Sci Rep* **11**, 4227 (2021).

28. J. Lengefeld, Y. Barral, Asymmetric segregation of aged spindle pole bodies during cell division: Mechanisms and relevance beyond budding yeast? *Bioessays* **40**, e1800038 (2018).

29. C. Stark *et al.*, BioGRID: a general repository for interaction datasets. *Nucleic Acids Res* **34**, D535-539 (2006).

30. E. D. Strome, X. Wu, M. Kimmel, S. E. Plon, Heterozygous screen in *Saccharomyces cerevisiae* identifies dosage-sensitive genes that affect chromosome stability. *Genetics* **178**, 1193-1207 (2008).

31. S. A. Nelson, A. M. Sanson, H. O. Park, J. A. Cooper, A novel role for the GTPase-activating protein Bud2 in the spindle position checkpoint. *PLoS One* **7**, e36127 (2012).

32. S. Soues, I. R. Adams, *SPC72*: a spindle pole component required for spindle orientation in the yeast *Saccharomyces cerevisiae*. *J Cell Sci* **111 ( Pt 18)**, 2809-2818 (1998).

33. J. V. Kilmartin, Purification of yeast tubulin by self-assembly in vitro. *Biochemistry* **20**, 3629-3633 (1981).

34. A. Rauch, E. Nazarova, J. Vogel, Analysis of microtubules in budding yeast. *Methods Cell Biol* **97**, 277-306 (2010).

35. A. Matsuura, M. Tsukada, Y. Wada, Y. Ohsumi, Apg1p, a novel protein kinase required for the autophagic process in *Saccharomyces cerevisiae*. *Gene* **192**, 245-250 (1997).

36. A. Matsui, Y. Kamada, A. Matsuura, The role of autophagy in genome stability through suppression of abnormal mitosis under starvation. *PLoS genetics* **9**, e1003245-e1003245 (2013).

37. D. Liakopoulos, J. Kusch, S. Grava, J. Vogel, Y. Barral, Asymmetric loading of Kar9 onto spindle poles and microtubules ensures proper spindle alignment. *Cell* **112**, 561-574 (2003).

38. M. Hotz *et al.*, Spindle pole bodies exploit the mitotic exit network in metaphase to drive their age-dependent segregation. *Cell* **148**, 958-972 (2012).

39. G. Pereira, T. U. Tanaka, K. Nasmyth, E. Schiebel, Modes of spindle pole body inheritance and segregation of the Bfa1p-Bub2p checkpoint protein complex. *EMBO J* **20**, 6359-6370 (2001).

40. J. Manzano-Lopez, L. Matellan, A. Alvarez-Llamas, J. C. Blanco-Mira, F. Monje-Casas, Asymmetric inheritance of spindle microtubule-organizing centres preserves replicative lifespan. *Nat Cell Biol* **21**, 952-965 (2019).

41. M. A. Juanes *et al.*, Spindle pole body history intrinsically links pole identity with asymmetric fate in budding yeast. *Curr Biol* **23**, 1310-1319 (2013).

42. Y. Wang *et al.*, Coiled-coil networking shapes cell molecular machinery. *Mol Biol Cell* **23**, 3911-3922 (2012).

43. D. Kozakov *et al.*, The ClusPro web server for protein-protein docking. *Nat Protoc* **12**, 255-278 (2017).

44. R. Chowdhury, M. F. Allan, C. D. Maranas, OptMAVEn-2.0: De novo design of variable antibody regions against targeted antigen epitopes. *Antibodies* **7**, 23 (2018).

45. R. Fraschini, D. Bilotta, G. Lucchini, S. Piatti, Functional characterization of Dma1 and Dma2, the budding yeast homologues of *Schizosaccharomyces pombe* Dma1 and human Chfr. *Mol Biol Cell* **15**, 3796-3810 (2004).

46. K. E. D'Aquino *et al.*, The protein kinase Kin4 inhibits exit from mitosis in response to spindle position defects. *Mol Cell* **19**, 223-234 (2005).

47. A. J. Bardin, R. Visintin, A. Amon, A mechanism for coupling exit from mitosis to partitioning of the nucleus. *Cell* **102**, 21-31 (2000).

48. J. N. Molk *et al.*, The differential roles of budding yeast Tem1p, Cdc15p, and Bub2p protein dynamics in mitotic exit. *Mol Biol Cell* **15**, 1519-1532 (2004).

49. J. K. Moore, S. D'Silva, R. K. Miller, The CLIP-170 homologue Bik1p promotes the phosphorylation and asymmetric localization of Kar9p. *Mol Biol Cell* **17**, 178-191 (2006).

50. L. Merlini *et al.*, Budding yeast Dma proteins control septin dynamics and the spindle position checkpoint by promoting the recruitment of the Elm1 kinase to the bud neck. *PLoS Genet* **8**, e1002670 (2012).

51. T. Yorimitsu, D. J. Klionsky, Atg11 links cargo to the vesicle-forming machinery in the cytoplasm to vacuole targeting pathway. *Mol Biol Cell* **16**, 1593-1605 (2005).

52. R. Krick *et al.*, Piecemeal microautophagy of the nucleus requires the core macroautophagy genes. *Mol Biol Cell* **19**, 4492-4505 (2008).

53. C. W. Lee *et al.*, Selective autophagy degrades nuclear pore complexes. *Nat Cell Biol* **22**, 159-166 (2020).

54. N. Matscheko, P. Mayrhofer, Y. Rao, V. Beier, T. Wollert, Atg11 tethers Atg9 vesicles to initiate selective autophagy. *PLoS Biol* **17**, e3000377 (2019).

55. A. K. Caydasi, B. Ibrahim, G. Pereira, Monitoring spindle orientation: Spindle position checkpoint in charge. *Cell Div* **5**, 28 (2010).

56. J. Kusch, A. Meyer, M. P. Snyder, Y. Barral, Microtubule capture by the cleavage apparatus is required for proper spindle positioning in yeast. *Genes Dev* **16**, 1627-1639 (2002).

57. F. C. Luca *et al.*, *Saccharomyces cerevisiae* Mob1p is required for cytokinesis and mitotic exit. *Mol Cell Biol* **21**, 6972-6983 (2001).

58. F. Meitinger *et al.*, Targeted localization of Inn1, Cyk3 and Chs2 by the mitotic-exit network regulates cytokinesis in budding yeast. *J Cell Sci* **123**, 1851-1861 (2010).

59. M. Shirayama, W. Zachariae, R. Ciosk, K. Nasmyth, The Polo-like kinase Cdc5p and the WD-repeat protein Cdc20p/fizzy are regulators and substrates of the anaphase promoting complex in *Saccharomyces cerevisiae*. *EMBO J* **17**, 1336-1349 (1998).

60. F. M. Yeong, H. H. Lim, U. Surana, MEN, destruction and separation: mechanistic links between mitotic exit and cytokinesis in budding yeast. *Bioessays* **24**, 659-666 (2002).

61. A. T. Vessoni, E. C. Filippi-Chiela, C. F. Menck, G. Lenz, Autophagy and genomic integrity. *Cell Death Differ* **20**, 1444-1454 (2013).

62. J. Cheng *et al.*, Centrosome misorientation reduces stem cell division during ageing. *Nature* **456**, 599-604 (2008).

63. J. A. Knoblich, Asymmetric cell division: recent developments and their implications for tumour biology. *Nat Rev Mol Cell Biol* **11**, 849-860 (2010).

64. M. A. Lancaster, J. A. Knoblich, Spindle orientation in mammalian cerebral cortical development. *Curr Opin Neurobiol* **22**, 737-746 (2012).

65. Y. M. Yamashita, A. P. Mahowald, J. R. Perlin, M. T. Fuller, Asymmetric inheritance of mother versus daughter centrosome in stem cell division. *Science* **315**, 518-521 (2007).

## Figures and figure legends

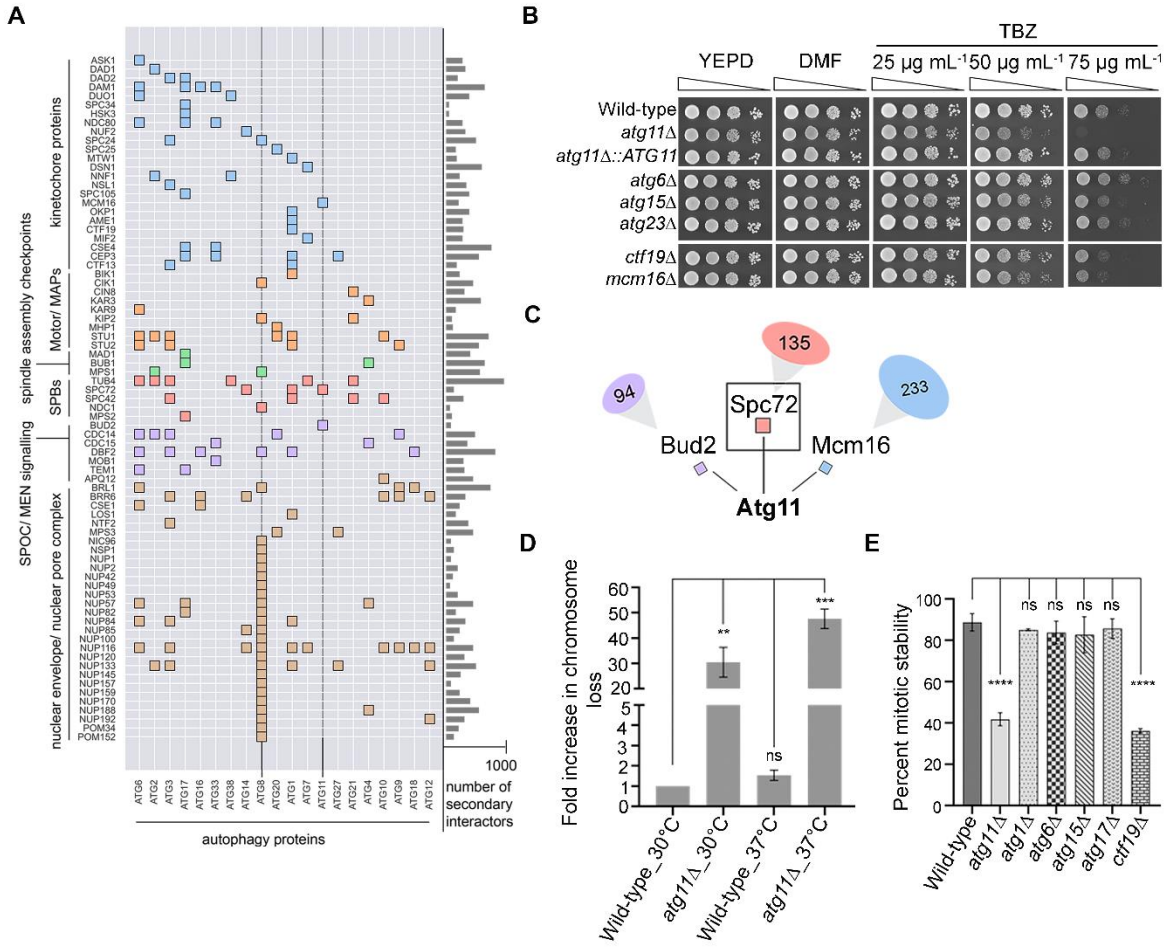


**Figure 1. Cells lacking Atg11 displays an increased rate of chromosome loss.** (A) Autophagy (Atg) proteins (*x*-axis) and their primary interactors (*y*-axis) are functionally clustered and shown. The marginal bar chart on the right indicates the number of secondary interactors of Atg proteins via each of the primary interactors. (B) Exponentially growing cells of wild-type, *atg11*Δ, *atg11*Δ*::ATG11*, *atg6*Δ, *atg15*Δ, *atg23*Δ, *ctf19*Δ, and *mcm16*Δ strains

were 10-fold serially diluted and spotted on YEPD, and YEPD plates containing dimethylformamide (DMF, solvent control) or increasing concentration of thiabendazole (TBZ) as indicated. Images were taken after incubation at 30°C for 2 days. (C) Primary (square boxes) and secondary (oval) interactors of Atg11 as reported in the latest curation of BioGRID (29). (D) Bar graph showing fold increase in chromosome loss in wild-type and *atg11*Δ strains at 30°C and 37°C. Error bar indicates standard deviation (SD), and statistical analysis was done using one-way ANOVA at $P<0.05$. (E) Mitotic stability of a monocentric plasmid was determined in wild-type, *atg11*Δ, *atg1*Δ, *atg6*Δ, *atg15*Δ, *atg17*Δ, and *ctf19*Δ strains. The assay was done with three independent sets of transformants. Statistical analysis was done using one-way ANOVA (****$P<0.0001$).

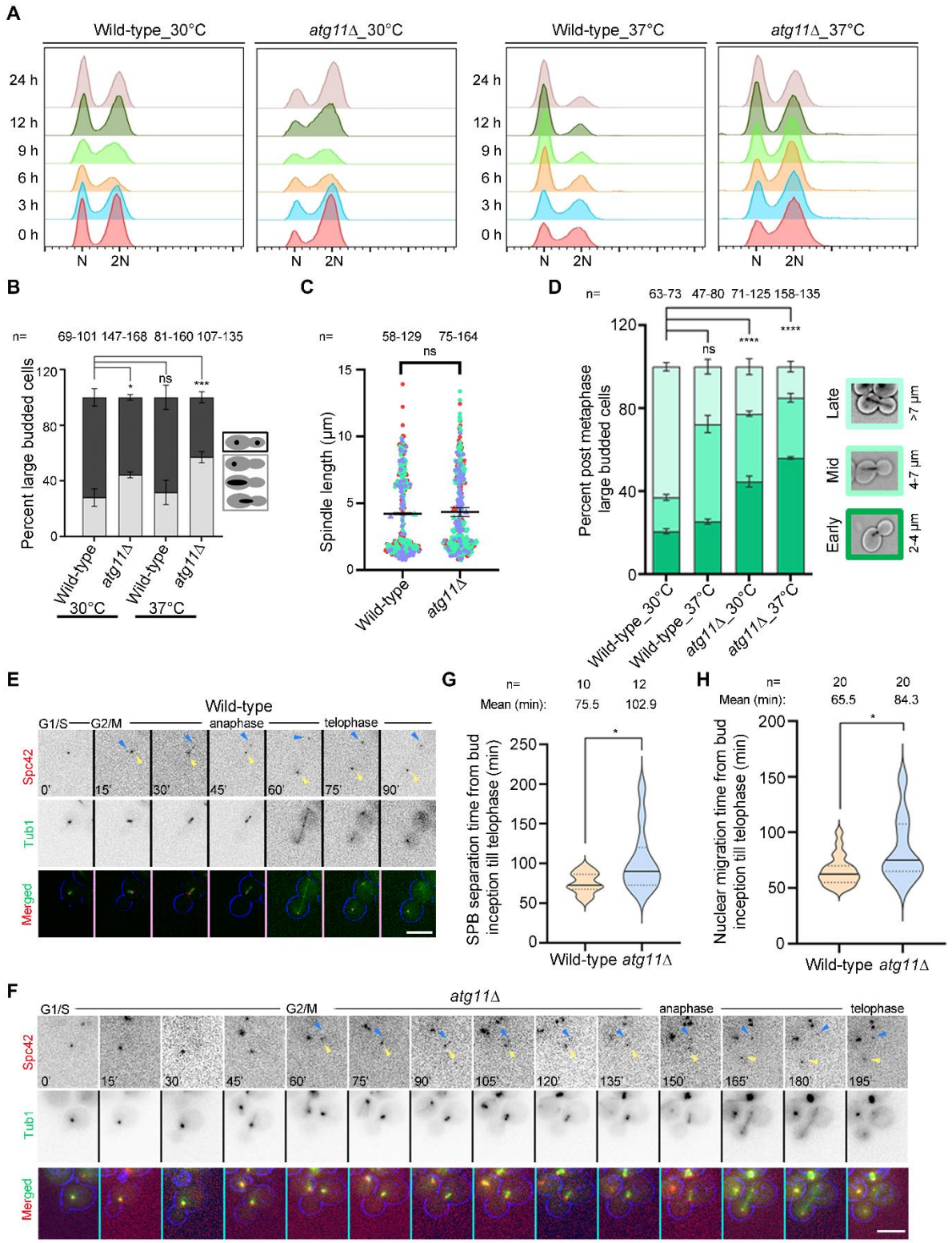


**Figure 2. The *atg11*Δ mutant cells show a delayed entry into anaphase.** (A) Flow cytometric to measure ploidy of the population of cells of indicated strains at 30°C and 37°C, at regulated intervals as shown. (B) Bar graph representing the percent of large-budded cells (budding index >0.6) having the nucleus either segregated (black) or unsegregated (grey) in wild-type

and *atg11*Δ cells at the indicated temperature. Error bars show mean ± standard error of deviation (SD) from three biological replicates. Cartoons show cellular morphology (grey), and chromatin mass (black) associated with the corresponding class. Statistical analysis was done using two-way ANOVA for multiple comparisons (**P=0.0182* and ****P=0.0001*). (C) A scatter plot displaying the spindle (GFP-Tub1) length in wild-type and *atg11*Δ mutant. Data represent mean ± standard error of the mean (SEM) from three independent experiments and calculated using unpaired *t*-test at *P*=0.05. (D) A bar graph representing the percent of post metaphase large-budded cells having early (2-4 μm), mid (4-7 μm), and late (>7 μm) anaphase spindle (GFP-Tub1) in wild-type and *atg11*Δ null mutant at 30°C and 37°C. n (wild-type_30°C 63-73; wild-type_37°C 47-80; *atg11*Δ_30°C 71-125; *atg11*Δ_37°C 58-135) represents the number of large-budded cells (budding index of >0.6) analyzed in three independent biological replicates. Error bars show mean ± SEM. Statistical analysis was done using two-way ANOVA for multiple comparisons at *P*=0.05. (E-F) A representative montage of the time-lapse image showing SPB (Spc42-mCherry) separation and spindle (GFP-Tub1) elongation in wild-type and *atg11*Δ cells respectively at 30°C. Scale bar 5 μm. Yellow and blue arrowheads mark the old and new SPB, based on fluorescence signal intensities, respectively. (G) A violin plot displaying the time taken for the completion of SPB separation between mother and daughter cells during the cell cycle from the inception of bud in strains as indicated. The number on top represents the average time taken for the completion of SPB separation. The continuous black line on the violin plot represents the median, while the dotted lines represent quartiles. The statistical significance was done using an unpaired *t*-test with Welch's correction at *P*=0.0398. (H) A violin plot displaying the time taken for the segregation of the nucleus in the two cells during the cell cycle from the bud inception in strains as indicated. The number on top represents the average time taken for the completion of nuclear migration. The statistical significance was done using an unpaired *t*-test with Welch's correction at *P*=0.0142.

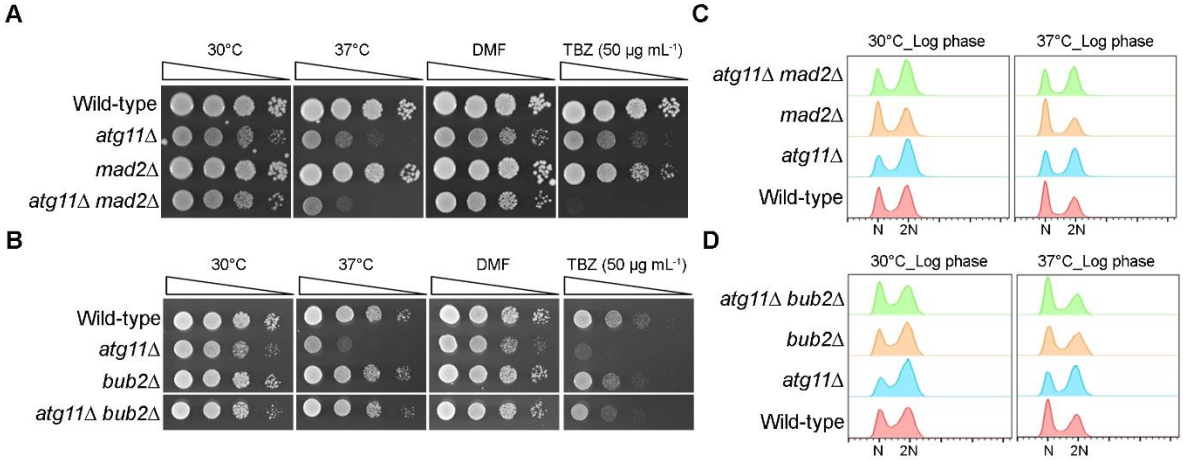


**Figure 3. Atg11 contributes to Bub2-mediated spindle positioning.** (A) Exponentially growing cells of wild-type, single and double mutants were 10-fold serially diluted and spotted on YEPD and YEPD plates containing DMF (solvent control) or thiabendazole (TBZ) at the indicated concentration. Plates were photographed after 48 h of incubation at 30°C or 37°C. (B) Exponentially growing cells of indicated strains were 10-fold serially diluted and spotted on YEPD and YEPD plates containing without the drug (DMF, solvent control) or in presence of TBZ. Plates were photographed after 33 h of incubation at 30°C or 37°C. (C and D) Flow cytometric analysis of cell cycle displaying the cellular DNA content of the indicated strains grown for 5 generations at 30°C or 37°C. The experiment was repeated three times using freshly streaked cultures.

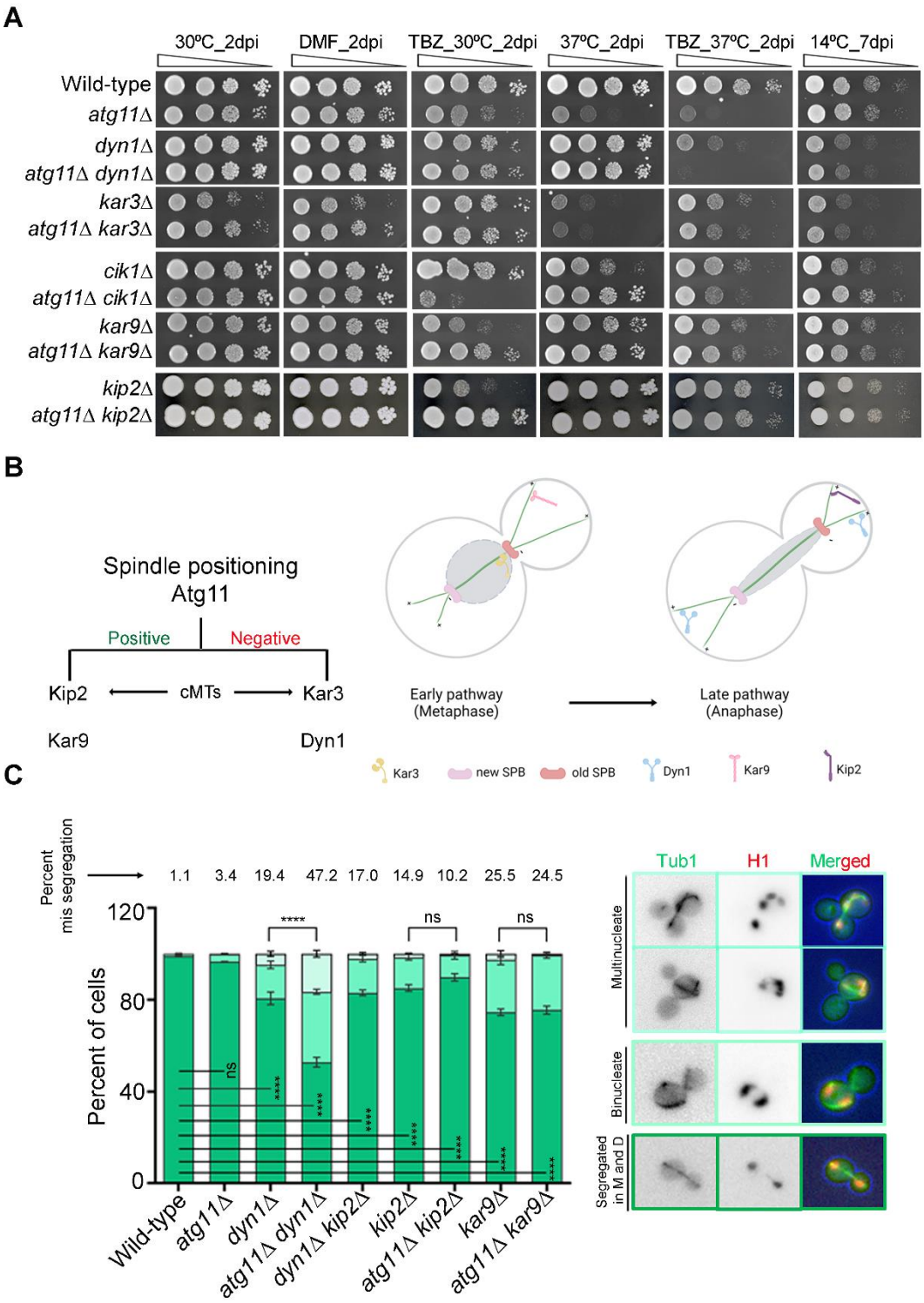


**Figure 4. Atg11 is required for proper spindle positioning.** (A) Growth assay of wild-type and *atg11*Δ with deletion mutants of kinesin-related motors and Atg11 interacting proteins at indicated temperature and in presence of TBZ. The cells were 10-fold serially diluted and spotted on YEPD, and YEPD containing TBZ. DMF was used as a no-drug control. Images

were taken after 2 days of incubation, except 7 days post-inoculation (dpi) for 14°C. (B) A model summarizing novel genetic interactions between Atg11 and Kip2 as well as Kar9 (positive) and with Kar3 as well as Dyn1 (negative). Kip2 and Kar3 regulate the length of cytoplasmic microtubules (cMTs), while Kar9 and Dyn1 regulate spindle positioning in metaphase (early pathway) and anaphase (late pathway) respectively. (C) Bar graph showing the percent of cells with segregated nuclei in the mother and daughter cells, mispositioned anaphase nuclei, and cells with more than one bud, multiple nuclei, or no nucleus. Error bars show mean ± standard error of the mean (SEM). Statistical analysis was done using two-way ANOVA for multiple comparisons at $P$=0.05.

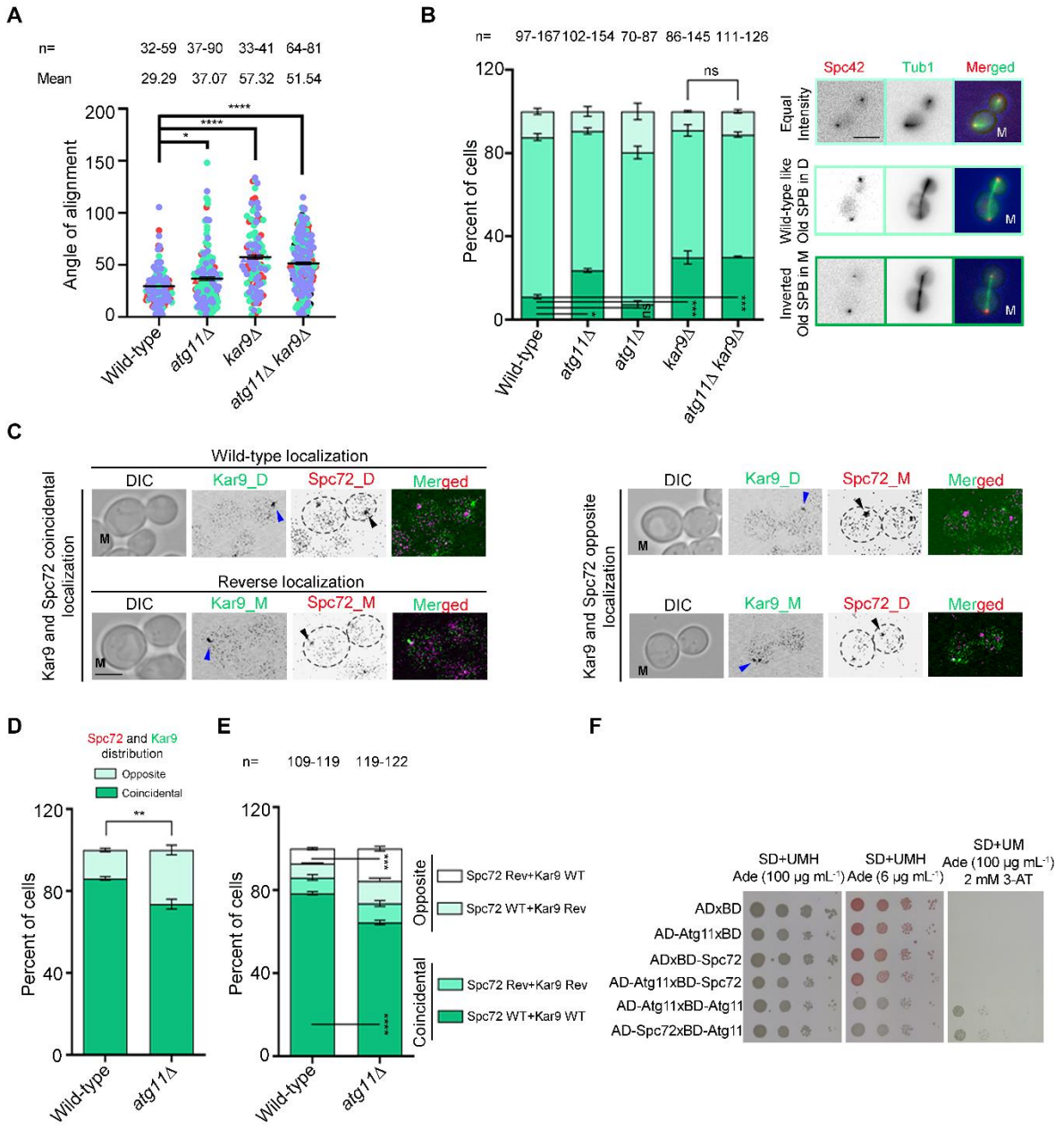


**Figure 5. The *atg11*Δ mutant exhibits inverted localization of Spc72 and Kar9 on the SPBs.** (A) The metaphase cells of wild-type, single or double mutants displaying a short bipolar spindle were analyzed for the angle of alignment along the mother-bud axis. The mean angle of alignment (black) represents data from three independent biological repeats. The number of cells analyzed is represented by n. Statistical analysis was done using one-way ANOVA at *P*=0.05. (B) Bar graph displaying percent of cells having reversed (old SPB in the mother cell), wild-type-like (old SPB in the daughter cell), or symmetric (equal intensity) SPB inheritance in the indicated strains based on Spc42-mCherry intensity. Representative images of above

mentioned SPB inheritance are shown. The number of cells analyzed from three independent biological replicates is mentioned as n. Statistical analysis was done using two-way ANOVA for multiple comparisons at $P$=0.05. Scale bar 5 μm. (C) Representative images displaying coincidental or opposite distribution of Kar9-GFP (green) and Spc72-mCherry (magenta) in wild-type and *atg11*Δ cells, exhibiting wild-type-like (asymmetric accumulation in the bud) or reversed (asymmetric accumulation in mother) localization of both the proteins. Asymmetric localization of Kar9-GFP and Spc72-mCherry is marked by blue and black arrowheads respectively. Scale bar 5 μm. (D, E) Bar graph representing the percent of cells displaying coincidental (dark green) and opposite (light green) Kar9-GFP and Spc72-mCherry localization (D). For each case, the wild-type and reversed distribution pattern are also further subclassified (E). The number of cells analyzed is represented by n. Error bars show mean ± standard error of the mean (SEM). Statistical analysis was done using two-way ANOVA at $P$=0.05. (F) Yeast-two hybrid (Y2H) assay in *S. cerevisiae* strains carrying the mentioned plasmid combinations was 10-fold serially diluted and spotted on SD minimal medium plates lacking Trp and Leu or Trp, Leu, and His supplemented with 2 mM 3-amino-1,2,4-triazole (3-AT) and grown at 30°C.

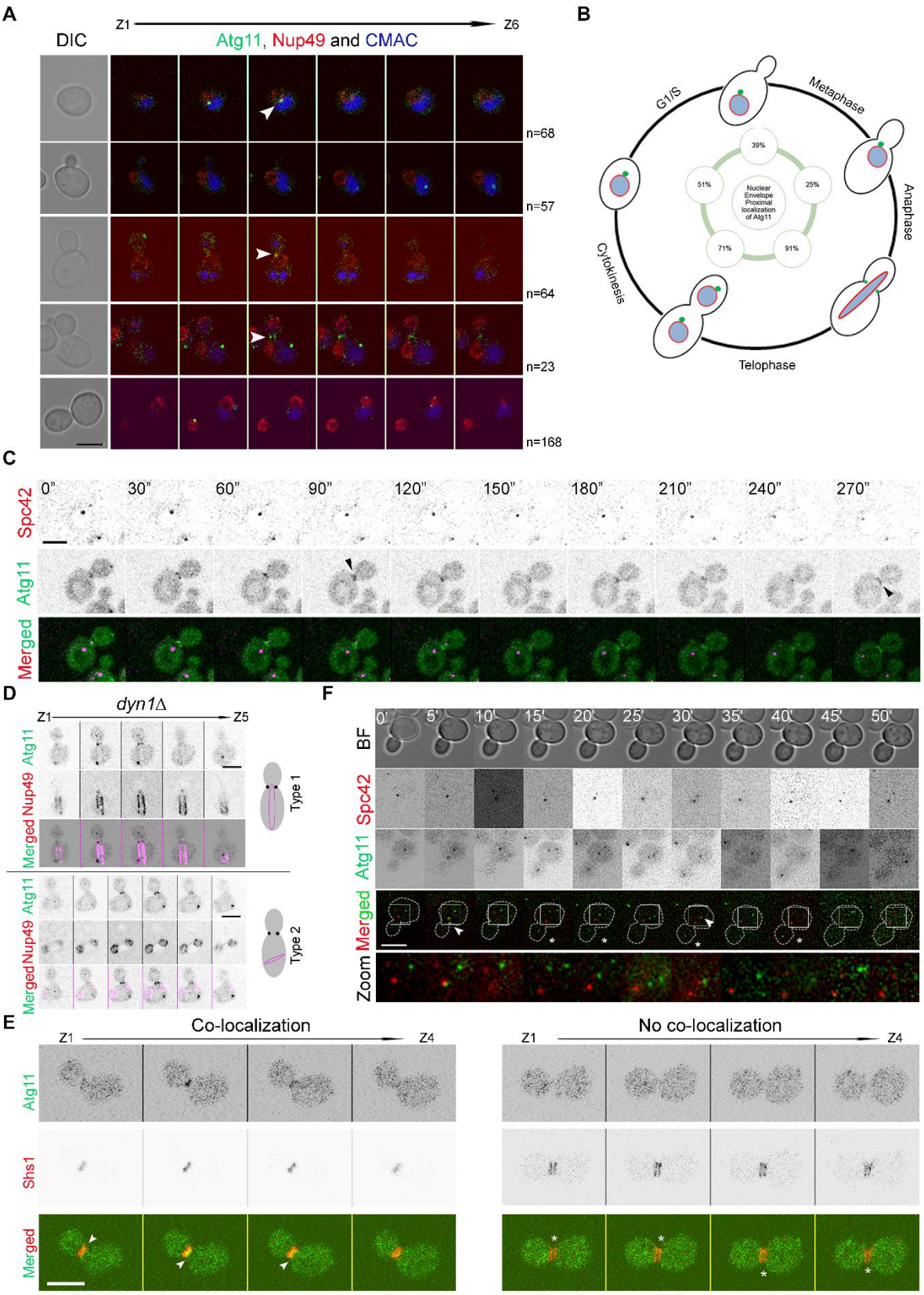


**Figure 6. Cell cycle-dependent localization of Atg11 with the nuclear envelope, at the bud neck and SPBs.** (A) Micrographs representing different focal planes showing co-localization (white arrowheads) of Atg11 (sfGFP-Atg11) with the nuclear envelope marker, Nup49-

mCherry at various stages of cell cycle in cells co-stained with the vacuolar lumen dye CMAC. The number of cells analyzed for each cell type is represented by n. Scale bar 6 μm. (B) Schematic showing percent co-localization of Atg11 with the nuclear envelope (NE) at various stages of the cell cycle. (C) A representative time-lapse montage showing bud-neck localization (black arrowheads) of Atg11 with the SPBs (Spc42-mCherry) during the cell cycle. Scale bar 5 μm. (D) Micrographs representing different focal planes revealing bud-neck localization of Atg11 with respect to the nuclear envelope, Nup49 (Nup49-mCherry) in dynein mutants having binucleated phenotype in the mother cell. Scale bar 5 μm. (E) Confocal micrographs representing different focal planes displaying co-localization of Atg11 with Shs1-mCherry marked with white arrowheads and loss of Atg11 localization from the bud-neck, marked with white asterisks. Scale bar 6 μm. (F) A representative time-lapse image of proximal localization of Atg11 with SPBs in wild-type cells having duplicated SPBs in mother cells followed for 50 min. Arrowheads, in white, show Atg11 being close first with the dSPB at 5 min, and later with the mSPB at 30 min. The asterisks show the movement of Atg11 in the daughter cell before the movement of daughter SPB (dSPB). Scale bar 6 μm.

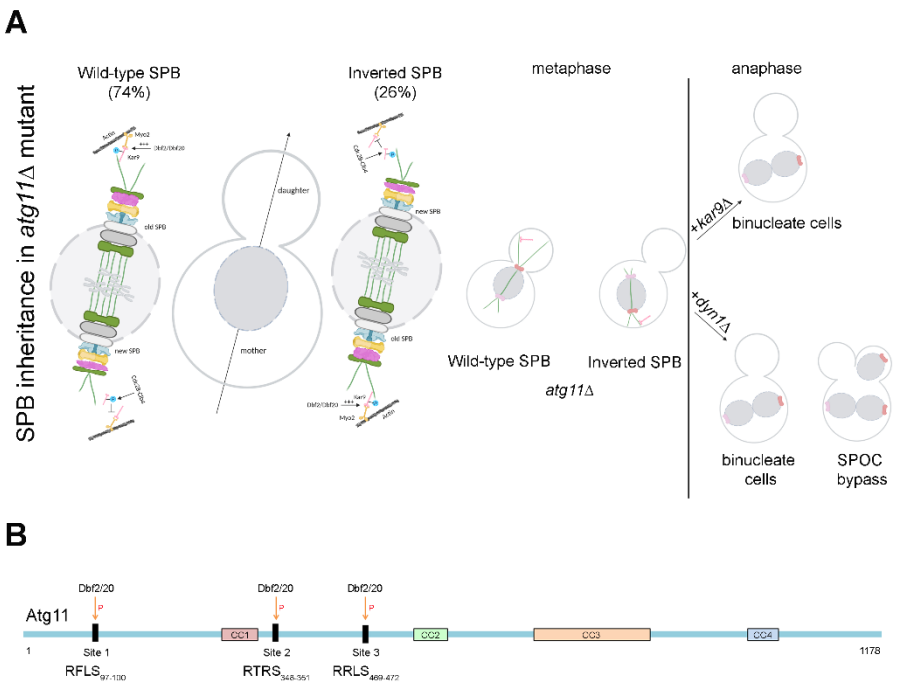


**Figure 7. Atg11 mediates asymmetric SPB inheritance crucial for spindle alignment in *S. cerevisiae*.** (A) Lack of Atg11 leads to the loss of Spc72 and Kar9 asymmetry, leading to SPB inheritance defect. The *atg11*Δ mutant displays spindle mispositioning during metaphase and shows a binucleate phenotype upon loss of Kar9, similar to the *kar9*Δ mutant. Loss of *ATG11* in *dyn1*Δ mutant displays a defect in spindle position checkpoint, leading to the formation of multinucleated cells. (B) Schematic of the Atg11 protein sequence depicting the four coiled-coil domains and consensus site, RXXS, for Dbf2/Dbf20. Analysis of the Atg11 protein sequence indicates the presence of three Dbf2/Dbf20 consensus sites (RXXS) at Ser100, Ser351, and Ser472.